Talk Presented at the ANL Heavy
Ion Symposium, Argonne, Ill.
March 13-21, 1973

LBL-1653
c.1

INELASTIC SCATTERING OF HEAVY IONS

F. D. Becchetti

March 1973

Prepared for the U.S. Atomic Energy
Commission under Contract W-7405-ENG-48

LBL-1653
c.1

DISCLAIMER

INELASTIC SCATTERING OF HEAVY IONS*

F. D. Becchetti
Lawrence Berkeley Laboratory
University of California
Berkeley, California 94720

I. INTRODUCTION

The inelastic scattering of heavy ions exciting low lying collective levels can be described as a "quasi-elastic" process since the energy, mass, and charge transfers are small or zero. The small energy ($Q \approx 0$) and charge transfers imply that the projectile orbits, incoming and outgoing, can be deduced from observation of the elastic scattering. Standard DWBA or CCBA would appear to be applicable since the mass transfer is zero and thus the no-recoil approximation need not be invoked. Furthermore, as we shall see, the angular distributions depend, in most cases, on the multipolarity of the transition. These features are in contrast to those for nucleon transfer between heavy ions. The interpretation of transfer reactions is plagued by uncertainties in optical model parameters and recoil effects in DWBA, and lack of L-dependence in the angular distributions.

In the following sections I will discuss: a) nuclear and Coulomb interference and the phase of the H. I. - nucleus interaction b) the shape of the H. I. optical potential and c) determination of deformation parameters. I will concentrate on inelastic scattering of "light" heavy ions (^{12}C, ^{16}O, etc.) on nuclei $A \geq 40$, at energies above the Coulomb barrier. The data are mostly from Copenhagen[1-3] (NBI) and Berkeley[4,5] (LBL). Inelastic scattering resonances are discussed elsewhere in these proceedings.

II. NUCLEAR AND COULOMB INTERFERENCE

Much information about the sign, shape and magnitude of nucleon-nucleon and nucleon-nucleus forces has been deduced from observation of scattering in the presence of the combined nuclear and Coulomb fields. The elastic scattering angular distributions exhibit oscillations which, in part, arise from the interference between nuclear and Coulomb scattering.

Interference effects are most pronounced when nuclear and Coulomb forces are comparable. Such is often the case for inelastic scattering of ^{3}He, alpha particles and heavy ions from nuclei. In DWBA, excitation of a collective level is described by the interaction (form factor)[6-8]

$$F_L(r) = F_L^C(r) + F_L^N(r) \tag{1}$$

where

$$F_L^C(r) = \frac{eZ_1}{2L+1} \frac{4\pi \sqrt{B(EL)}}{r^{L+1}} \tag{2}$$

and

$$F_L^N(r) = \beta_L^N (V_R R_R \frac{df}{dr} + iW_I R_I \frac{dg}{dr}) \tag{3}$$

In these equations, L is the multipolarity of the transition and $F_L^C(r)$ and $F_L^N(r)$ are the Coulomb and nuclear excitation forces, respectively. The latter is proportional to the derivative of the optical potential, $V_R\, f(r) + iW_I\, g(r)$, which describes the elastic scattering. β_L^N is the potential deformation due to the target nuclear deformation (target excitation). Since the optical potential is usually attractive ($V_R < 0$), as well as absorptive ($W_I < 0$) there is a point for which $\mathrm{Re}(F_L(r)) = 0$. This results in a minimum in the inelastic scattering angular distribution (or excitation function).[7,8] Such destructive interference has been observed in (^{3}He,^{3}He'), (α,α') and (^{6}Li,^{6}Li'), although the effects are often small.[9,10,11]

In Fig. 1 we show data[4] (LBL) for $^{208}Pb(^{16}O,^{16}O')^{208}Pb$ (g.s., 3^-, 5^-, 2^+) as a function of angle (E = 104 MeV) while in Fig. 2 we show data[3] (NBI) for $^{88}Sr(^{16}O,^{16}O')^{88}Sr$ (g.s., 2^+, 3^-) as a function of energy ($\theta_L = 175°$). Two regions are observed, respectively: small angles (low energies) for which $\sigma_{el}/\sigma_R \approx 1$ and $\sigma_{inel}(\theta,E)$ depends on L (and/or Q), and large angles (high energies) where $\sigma_{inel}(\theta,E)$ is nearly L-independent. These features can be qualitatively understood in terms of interference between nuclear and Coulomb scattering of ions whose orbits are described semi-classically ($\eta >> 1$, $L << kR$). In such a picture the inelastic scattering can be written as[8]

$$\sigma_{inel}(\theta,E) = P_L \, \sigma_{el}(\theta,E) \tag{4}$$

where P_L is the inelastic scattering probability and $\sigma_{el}(\theta,E)$ is the elastic scattering. Furthermore one can show that[12]

$$P_L \propto |F_L(D)|^2 \tag{5}$$

where $D(\theta,E)$ is the distance of closest approach, which for Coulomb orbits is given by

$$D(\theta,E) = (Z_1 Z_2 / 2E_{c.m.})\,(1 + \csc \theta/2) \tag{6}$$

We illustrate this in Fig. 3 where we show $\sigma_{inel}/\sigma_{el}$ for ^{16}O, $^{12}C + {}^{96}Zr(2^+ + 3^-)$ versus $|F_L(D)|^2$ for L = 3 (the main component of the states excited).[2] In the region r, D > 13 fm (small θ, low E) Coulomb forces dominate and P_L and σ_{inel} are L-dependent ($F_L^C(D) \propto 1/D^{L+1}$) whereas for r, D < 11 fm (large θ, high E), nuclear forces and absorption (L independent) dominate. The strong absorption dampens any oscillations r, D < 11 fm. The minimum in the inelastic cross section occurs at $D(\theta,E)$ such that $Re(F_L^C(D) + F_L^N(D)) \approx 0$. It is interesting to note that the elastic scattering at the corresponding $D(\theta,E)$ exhibits constructive interference (Figs. 1, 2). Since the relation (6) neglects the distortion of the real potential, the minimum in $\sigma_{inel}(D)$ appears to shift

slightly with E and/or θ. This is shown in Fig. 4a for $^{58}Ni(^{16}O,^{16}O')^{58}Ni(2^+)$ measured[3] as functions of θ(E = 44, 50, 60 MeV) and E(θ = 60°, 75°, 90°, 175°). The maximum in $\sigma_{el}(D)/\sigma_R(D)$ also shifts accordingly,[3] as can be seen in Fig. 4b. The effect of the real potential on the projectile orbit can be included in a semi-classical model by calculation of the deflection function.[8] The absorption can also be treated.[8] Figure 5 compares the results of semi-classical and quantum mechanical calculations[8] for $^{58}Ni + ^{16}O$. Except for the region of strong absorption (where $\sigma_{inel} \to \sigma_{el}$) both methods give similar results, although the use of the semi-classical method may be advantageous when many inelastic transitions must be coupled.[8]

In the discussions above we have assumed the validity of the collective model (Eqs. 1-3). It has been pointed out, however, that nuclear - Coulomb interference can be used as a sensitive probe of the phase of the nuclear inelastic form factor.[13] Thus one may rewrite (3) as

$$F_L^N(r) = \beta_L^N \, U e^{i\alpha} \, R \, \frac{df}{dr}(r) \qquad (7)$$

The determination of the phase α is necessary to facilitate comparisons with form factors calculated using microscopic models.[13] In nucleon-nucleus inelastic scattering $F_L^N(r) >> F_L^C(r)$ and as a consequence the shape and magnitude of σ_{inel} are nearly independent of α. Such is not usually the case for the inelastic scattering of heavy ions.

In Fig. 6 we show DWBA calculations[4] for $^{208}Pb(^{16}O,^{16}O')^{208}Pb(3^-)$. The calculations for θ > 80° are relatively insensitive to α (since $F_L^C(D) \ll F_L^N(D)$) and $\beta_L^N U$ can be determined by fitting the magnitude of $\sigma_{inel}(\theta)$). Similarly the forward angle data determines B(EL). The phase α can then be adjusted to fit the interference pattern. The result[4] for the data shown is α = 30° ± 15°. This is in very good agreement with the collective model value α = 20° deduced from the optical model potential used to fit the elastic scattering

($\alpha = \tan^{-1} |W_I/V_R|$ if $f(r) = g(r)$). The phases determined from nuclear-Coulomb interference in (α,α'), $(^3He,^3He')$ and $(^{16}O,^{16}O')$ on ^{208}Pb are all consistent[10,11,13] with the collective model which requires deformation of both the real and imaginary parts of the optical potential. The phase α will in general depend on bombarding energy since the ratio W_I/V_R will. Thus $\alpha \to 0^\circ$ as $E \to E_{\text{Coulomb Barrier}}$ $(W_I \to 0)$.

III. DETERMINATION OF OPTICAL MODEL POTENTIAL

The optical potential for heavy ions is often not determined very well from elastic scattering. This is due to the dominance of Coulomb forces at large projectile separation and strong absorption which occurs for close approaches. This can be seen by displaying the optical potentials and elastic scattering[2] vs. $D(\theta,E)$, as shown in Figs. 7a and 7b. The potentials $V_R(r)$ and $W_I(r)$ are accurately determined only in the region $r > 9$ fm ($>R_R,R_I$). In this region the potentials satisfy the Igo relation[14] $V(r) \to V \exp(R/a)$ $\exp(-r/a) = C(a) \exp(-r/a)$. Thus the diffuseness parameter determines the potential shape. Recent analyses[2,3] of elastic scattering of ^{16}O and ^{12}C ions from nuclei $A \geq 40$ indicate $a_I \leq a_R \leq 0.6$ fm. The analysis of some transfer reaction data requires[16] $a_I \approx 0.6$ fm. The optical potentials generated by folding a nucleon-nucleus optical potential with the projectile density have[8,17] a_R, $a_I \gtrsim 0.6$ fm. It is possible to obtain a not unreasonable fit to elastic scattering data with a folded-type potential which has $a_R = a_I = 1$ fm (set IV, Figs. 7a and 7b).

Heavy ion inelastic scattering, however, is very sensitive to the potential shape since the derivative of the optical potential enters in the form factor (Eq. 3). This is shown in Fig. 8 for $^{16}O + ^{58}Ni$. The solid curve represents a calculation[3] with $a_R = 0.53$ fm and $a_I = 0.38$ fm while the dash

curve[2] is for $a_R = a_I = 1$ fm. Collective model phases were used for the calculations shown. It can be seen that a diffuse nuclear potential does not produce enough structure compared to the observed interference (this feature is relatively insensitive to α in this case). Similiar results have been obtained for other nuclei.[2] The analyses of nuclear-Coulomb interference indicate $a_I \lesssim a_R < 0.6$ fm.

Although the angular distributions for excitation of low lying levels are reproduced quite well by DWBA (see Figs. 1 and 2) there are indications that the calculations for very inelastic scattering (Ex >> 0, Q << 0) are shifted back in angle with respect to the data[2,4] (see Fig. 1). The observed shift with Q-value is very similiar to that observed for transfer reactions, where it is observed[16,18] that transfer with non quasi-elastic Q values ($Q \neq Q_{opt}$) are not fit by DWBA without parameter adjustments. The observation of this effect in inelastic scattering indicates that this phenomenon is associated with orbit mismatch and/or channel coupling and not problems associated with recoil, the transfer form factor, or mass and charge transfers per se. More H.I. inelastic data Ex >> 0 would be useful in further clarifying this problem.

IV. DEFORMATION MEASUREMENTS

The spectroscopic quantities obtained via super-Coulomb H.I. inelastic scattering are the E.M. transition rates B(EL) and potential deformations β_L^N (Eqs. 2 and 3). In practice, however, states Ex >> 0 and L >> 0 are excited mostly by nuclear excitation, owing to the rapid decrease of Coulomb excitation with L and Q. Therefore, transitions to states $L \lesssim 3$ and $Ex \lesssim 3$ MeV usually exhibit the most nuclear-Coulomb interference and can be used to measure simultaneously B(EL) and β_L^N. The quantity B(EL) is a measure of the target charge deformation (β_L^C) while β_L^N is a measure of the target mass deformation, β_L (in first order $\beta_L^N R_{OM} = \beta_L R$ where R_{OM} is the potential radius and R is the target radius).[19]

It has been observed that the charge and mass deformations deduced from different measurements (Coulomb excitation, (p,p'), (α,α'), etc.) often differ substantially.[19] One would like to correlate these differences with isospin, etc., however it is often not certain whether the observed effects are meaningful or merely reflect experimental and theoretical uncertainties (such as normalization problems). H.I. inelastic scattering can yield determinations of charge and mass deformations from a single experiment. This is illustrated in Fig. 9 for the first 2^+ states in several nuclei. Shown are the charge (β_2^C) and mass (β_2) deformations deduced from B(E2) and β_2^N values measured with ($^{16}O,^{16}O'$) compared with those deduced from separate measurements (in some cases average values). The agreement between the H.I. results and other measurements is good. The results shown indicate that $\beta_2^C \gtrsim \beta_2$ for the nuclei shown, except perhaps ^{48}Ca. In Table I we compare results obtained[4] from $^{208}Pb(^{16}O,^{16}O')$, E = 104 MeV (Fig. 1) with those[21-26] from (e,e'), (p,p'), (α,α'), and ($^3He,^3He'$). The light ion results are not very self-consistent, whereas the H.I. results have $\beta_L^C > \beta_L (G_{EL} > G_L)$. It can be seen from Table I that apparent differences in E.M. and nuclear transition rates (G_{EL} and G_L) can arise from higher-order effects in Coulomb excitation (e.g. reorientation) which are not included in a simple treatment (Eq. 2).

The results shown in Fig. 9 and Table I are for spherical nuclei. Recent technological advancements make it possible to study H.I. scattering from deformed nuclei at high bombarding energies with adequate energy resolution.[27] An example is given in Fig. 10 where a ^{12}C spectrum from $^{154}Sm(^{12}C,^{12}C')$, E = 78 MeV is shown.[5] Members of the g.s. rotational band (2^+, 4^+, 6^+, . . .) are excited with cross sections comparable to those for light ions.[28] It is hoped that such experiments will give information on the effects of the projectile size on measurements of high potential moments

(β_4,β_6) and resolve ambiguities that now exist between Coulomb excitation and (α,α') measurements. The quantitative interpretation of H.I. inelastic scattering from deformed nuclei must await the extension of coupled channels calculations (CCBA) to include energetic heavy ions.

V. SUMMARY

It is hoped that the preceding illustrations have shown that heavy-ion inelastic scattering at energies above the Coulomb barrier can be used to obtain information about the H.I.-nucleus interaction and nuclear shapes, and provide knowledge valuable for the interpretation of other heavy ion reactions.

REFERENCES

*Work performed under the auspices of the U. S. Atomic Energy Commission.

1. F. Videbaek, I. Chernov, P. R. Christensen, and E. E. Gross, Phys. Rev. Letters 28, 1072 (1972).
2. F. D. Becchetti, P. R. Christensen, V. I. Manko, and R. J. Nickles (to be published in Nucl. Phys.).
3. P. R. Christensen, I. Chernov, E. E. Gross, R. Stokstad, and F. Videbaek (submitted to Nucl. Phys.)
4. F. D. Becchetti, D. G. Kovar, B. G. Harvey, J. Mahoney, B. Mayer, and F. G. Pühlhofer, Phys. Rev. C6, 2215 (1972).
5. D. L. Hendrie, B. G. Harvey, H. Homeyer, D. G. Kovar, and W. von Oertzen, B.A.P.S. Washington meeting, 1973 and private communication.
6. R. H. Bassel, G. R. Satchler, R. M. Drisko, and E. Rost, Phys. Rev. 128, 2693 (1962).
7. C. Leclercq-Willian, Nuclear Reactions Induced by Heavy Ions, eds. W. Hering and R. Bock (North Holland, 1970). p. 453.
8. R. A. Broglia, S. Landowne, and S. Winther, Phys. Letters 40B, 293 (1972).
9. B. Wakefield, et al., Phys. Letters 31B, 56 (1970); R. J. Pryor, et al., Phys. Letters 31B, 26 (1970); F. T. Baker, et al., Phys. Letters 40B, 355 (1972); V. I. Chuev, et al., Phys. Letters 42B, 63 (1972).
10. F. T. Baker and R. Tickle, Phys. Letters 32B, 47 (1970).
11. F. Todd Baker and Robert Tickle, Phys. Rev. C5, 544 (1972).
12. P. J. Siemens and F. D. Becchetti, Phys. Letters 42B, 389 (1972).
13. G. R. Satchler, Phys. Letters 33B, 385 (1970); J. Y. Park and G. R. Satchler, Particles and Nuclei, 1, 233 (1971).
14. G. Igo, Phys. Rev. 115, 1665 (1959).
15. J. S. Eck, R. A. LaSalle, and D. A. Robson, Phys. Rev. 186, 1132 (1969); M. C. Bertin, et al., Nucl. Phys. A167, 216 (1971); B. C. Robertson, J. T. Sample, D. R. Goosman, K. Nagatani, and K. W. Jones, Phys. Rev. C4, 2176 (1971); A. W. Obst, D. L. McShan and R. H. Davis, Phys. Rev. C6, 1814 (1972). M. C. Lemaire, to be published in Physics Reports.
16. G. C. Morrison, H. J. Körner, L. R. Greenwood, and R. H. Siemssen, Phys. Rev. Letters 28, 1662 (1972).
17. S. G. Kadmenskii, et al., Yad Fiz. 10, 730 (1969). [(English transl.: Soviet J. Phys. 10, 422 (1970)].
18. P. R. Christensen, V. I. Manko, F. D. Becchetti, and R. J. Nickles, to be published in Nucl. Phys. D. Kovar, elsewhere in these proceedings.
19. A. M. Bernstein, in Adv. in Nucl. Phys., eds. M. Baranger and E. Vogt, 3, 325 (1969).
20. Compilation from Refs. 2, 3, 19, and P. H. Stelson and L. Grodzins, Nucl. Data 1, 21 (1966).
21. J. F. Ziegler and G. A. Peterson, Phys. Rev. 165, 1337 (1968).
22. A. R. Barnett and W. R. Phillips, Phys. Rev. 186, 1205 (1969).
23. J. Saudinos, G. Vallois, O. Beer, M. Gendrot, and P. Lopato, Phys. Letters 22, 492 (1966).
24. A. Scott and M. P. Fricke, Phys. Letters 20, 654 (1966).
25. J. Alster, Phys. Letters 25B, 459 (1967).
26. G. Bruge, J. C. Faivre, H. Farraggi and A. Bussiere, Nucl. Phys. A146, 597 (1970).
27. See for example: B. G. Harvey, et al., Nucl. Instr. Method 104, 21 (1972) and references therein.

28. B. G. Harvey, D. L. Hendrie, O. N. Jarvis, J. Mahoney, and J. Valentin, Phys. Letters 24B, 43 (1967).

Table I. Transition probabilities for states in ^{208}Pb.

		$(^{16}O,^{16}O')$[a]			(e,e')[b]	Coul. Ex[c]	(p,p')[d]	(p,p')[e]	(^{3}He,^{3}He')[f]	(α,α')
Ex(MeV)[i]	J^{π}[j]	β_L^N[k]	β_L[k]	G_L[l]	G_{EL}	G_{EL}	G_L	G_L	G_L	G_L
2.62	3^-	0.060	0.085	20 ± 4[m]	39.5±2	32±2	19.5	35.8	19.2	41.1±4.1[g]
				(25 ± 4)[n]		(24 ± 2)[o]				19.6[h]
3.20	5^-	0.036	0.051	8 ± 2[m]	14±5		8.1	10.7	3.5	14.1±1.6[g]
4.10	2^+	0.030	0.043	5 ± 1[m]	8.1±0.5		4.6	9.4	4.9	8.0±0.8[g]
4.31	4^+				26±2		6.4		5.2	14.8±1.6[g]

[a] Collective model analysis with optical potential: $U(r) = (V+iW)(1+\exp\frac{r-R}{a})^{-1}$ with V = −40 MeV, W = −15 MeV, $R = 1.31\,(A_1^{1/3} + A_1^{1/3})$ fm, a = 0.45 fm (see Fig.1)

[b] Ref. 21.

[c] Ref. 22; Coulomb excitation including reorientation, $E_{^{16}O}$ = 69.1 MeV, E_α = 17.5 - 19 MeV (Q = −1.3 b).

[d] Ref. 23, E_p = 24.6 MeV.

[e] Ref. 24, E_p = 40 MeV.

[f] Ref. 11, $E_{^3He}$ = 43.7 MeV.

[g] Ref. 25, E_α = 42 MeV.

[h] Ref. 26, E_α = 44 MeV.

[i] Measured in this experiment (± 50 keV).

[j] From Ref. 23.

[k] β_L^N is the potential deformation and β_L is the target mass deformation, as deduced from the deformation lengths (see text).

[l] $G_L \equiv B(L)/B_{sp}(L)$. Estimated errors are shown. $G_L = Z^2(3+L)^2\beta_L^2/4\pi(2L+1)$ where β_L is the mass (G_L) or charge (G_{EL}) deformation of the target.

[m] B(EL) from (e,e') of Ref. 21 (see Eq. (2)).

[n] B(EL) from $G_{EL} = G_L$ and adjusting G_L to fit the data.

[o] Deduced from the $^{16}O + ^{208}Pb$ data presented in Ref. 22 but neglecting reorientation terms (Q = 0 b).

LBL-1653

Figure Captions

Fig. 1. Angular distributions for $^{208}Pb(^{16}O,^{16}O')$, E_L = 104 MeV (Ref. 4). The curves are DWBA calculations for nuclear + Coulomb excitation (parameters given in Table I). The DWBA program DWUCK (P. D. Kunz, unpublished) was used.

Fig. 2. Excitation functions for $^{88}Sr(^{16}O,^{16}O')$, $\theta_L = 175°$ (Ref. 3). The curves are DWBA calculations.

Fig. 3. Top: The inelastic scattering probability of ^{16}O and ^{12}C from ^{96}Zr vs. $D(\theta)$ compared with a DWBA calculation. Bottom: The square of the form factor vs. separation (Ref. 2).

Fig. 4a. Ratio of inelastic (1.45 MeV) to elastic scattering of ^{16}O from ^{58}Ni as a function of the classical distance of closest approach (Eq. 6). This figure summarizes the data from four excitation functions and three angular distributions (Ref. 3). The curves are drawn to guide the eye.

Fig. 4b. Elastic scattering of ^{16}O from ^{58}Ni divided by the Rutherford cross section, as a function of the classical distance of closest approach (Eq. 6). This figure summarrizes the data from four excitation functions and three angular distributions (Ref. 3). The curves are drawn to guide the eye.

Fig. 5. A comparison of semi-classical and DWBA calculations for ^{16}O + ^{58}Ni (Refs. 1 and 8).

Fig. 6. Top: DWBA calculations for excitation due to Coulomb forces ($F_L(r) = F_L^C(r)$) or nuclear forces ($F_L(r) = F_L^N(r)$). Bottom: DWBA calculations for combined Coulomb and nuclear excitation as a function of the phase factor $\alpha(= \tan^{-1}|W_I/V_R|$, Eq. 7).

Fig. 7a. Left: The real part of the optical potentials which fit ^{16}O + ^{96}Zr elastic scattering (Ref. 2). Note that the origin starts at r = 4 fm. $V_C(r)$ is the Coulomb potential. Right: The elastic data for ^{16}O + ^{96}Zr

at 49(•) and 60(o) MeV as ratio to Rutherford scattering, versus $D(\theta)$ (Eq. 6). The curves are optical model calculations for the potentials indicated (E_L = 60 MeV).

Fig. 7b. Same as Fig. 6 but for the absorptive part of the OM potential.

Fig. 8. Elastic and inelastic scattering of $^{16}O + ^{58}Ni$ (Ref. 3). The solid curves are DWBA calculations with $a_I = 0.38$, $a_R = 0.53$ (Ref. 3) while the dot-dashed curves are for a folded-type potential, $a_R = a_I = 1$ fm (Ref. 2).

Fig. 9. Quadrupole charge (β_2^C) and mass deformations (β_2) deduced from ($^{16}O,^{16}O'$), ((•) Ref. 2, (▲) Ref. 3, (▼) Ref. 4) compared with other measurements ((o) Ref. 20).

Fig. 10. ^{12}C spectrum from $^{152}Sm + ^{12}C$, E_L = 78 MeV (Ref. 5). The positions of states in the g.s. rotational band are indicated (Ref. 28).

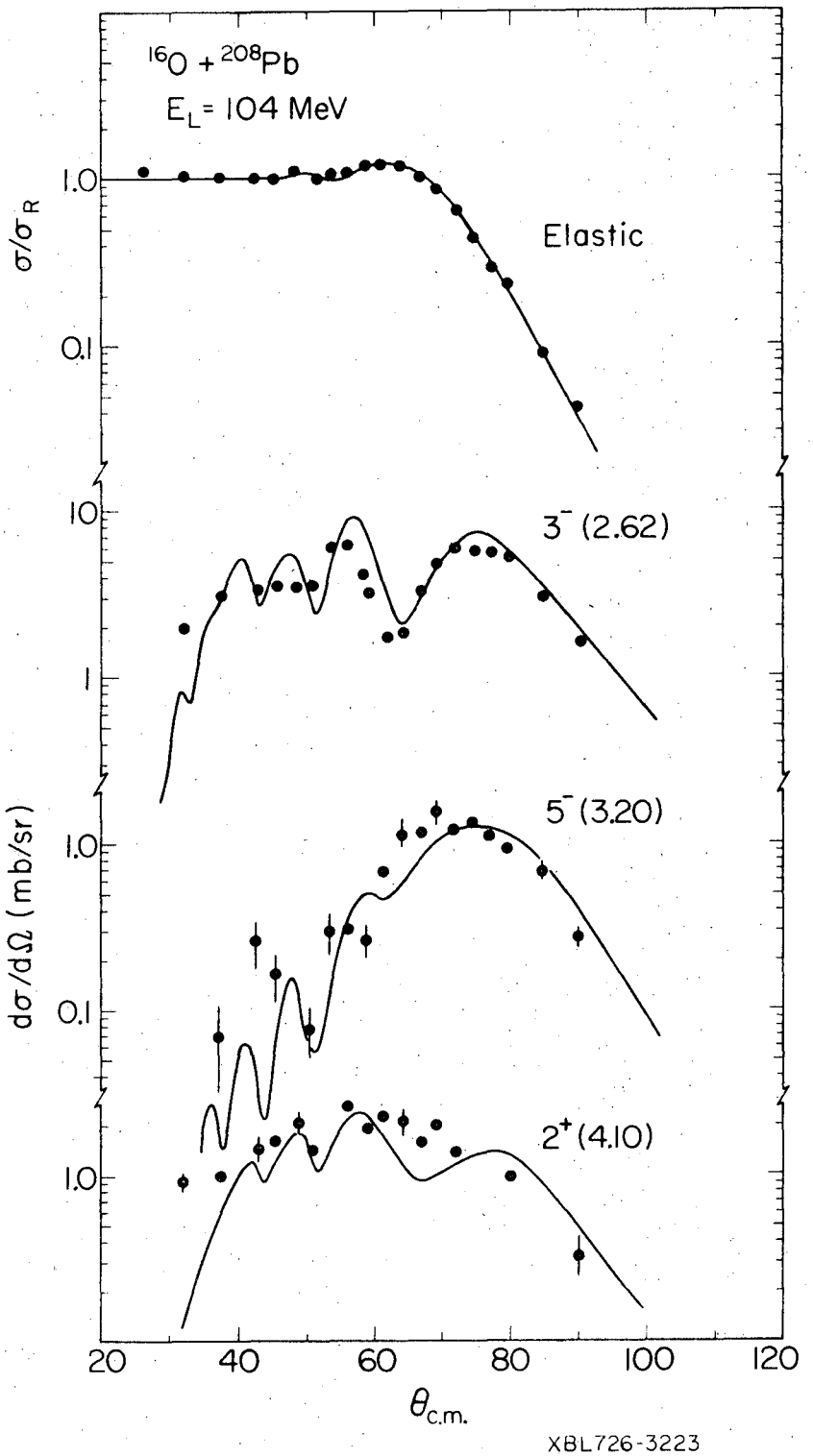
$^{16}O + ^{208}Pb$
E_L = 104 MeV
Elastic
3^- (2.62)
5^- (3.20)
2^+ (4.10)
σ/σ_R
$d\sigma/d\Omega$ (mb/sr)
$\theta_{c.m.}$
XBL726-3223

Fig. 1

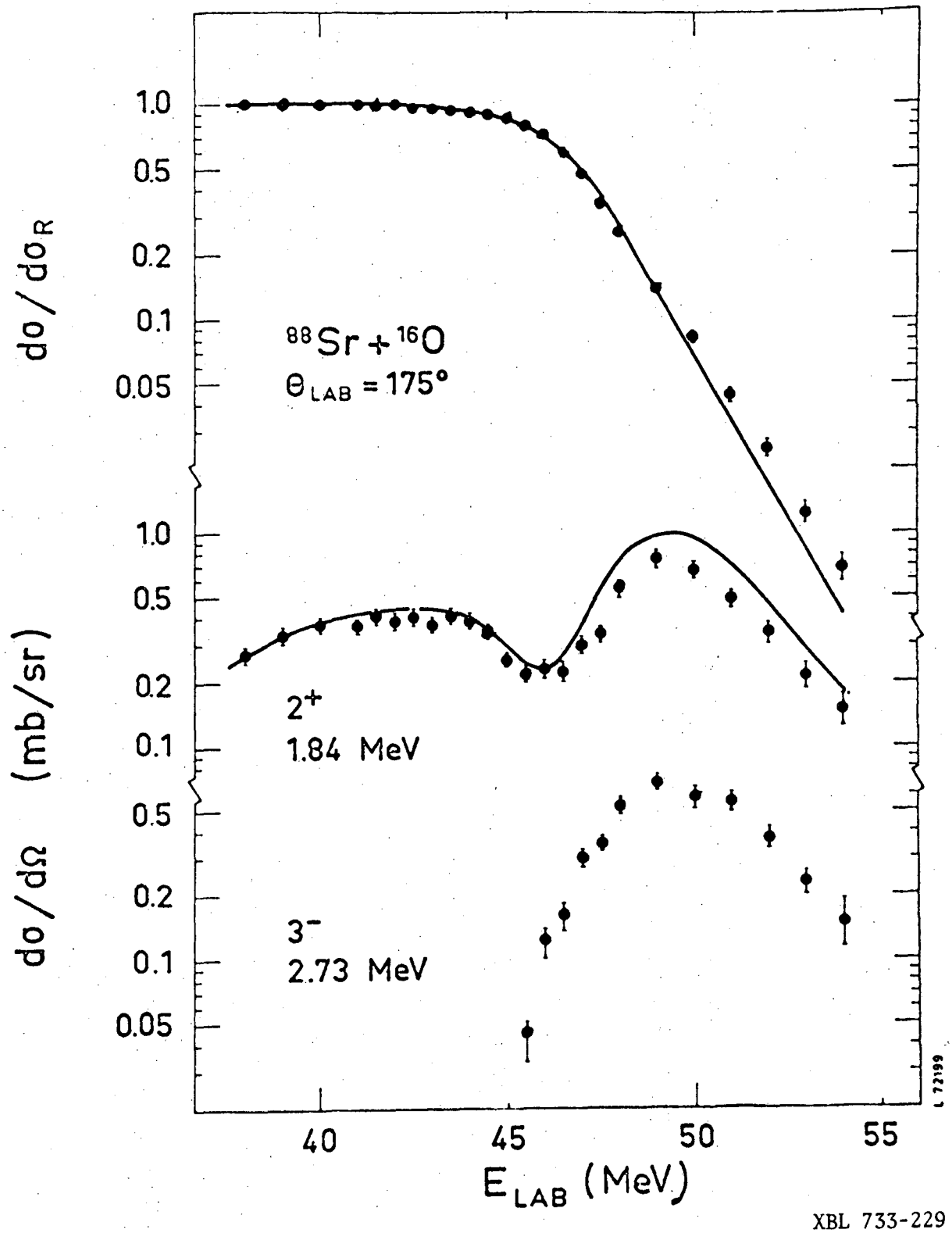
dσ/dσR
1.0
0.5
0.2
0.1
0.05
88Sr + 16O
θLAB = 175°
dσ/dΩ (mb/sr)
1.0
0.5
0.2
0.1
0.5
0.2
0.1
0.05
2+
1.84 MeV
3−
2.73 MeV
40
45
50
55
ELAB (MeV)
XBL 733-229

Fig. 2

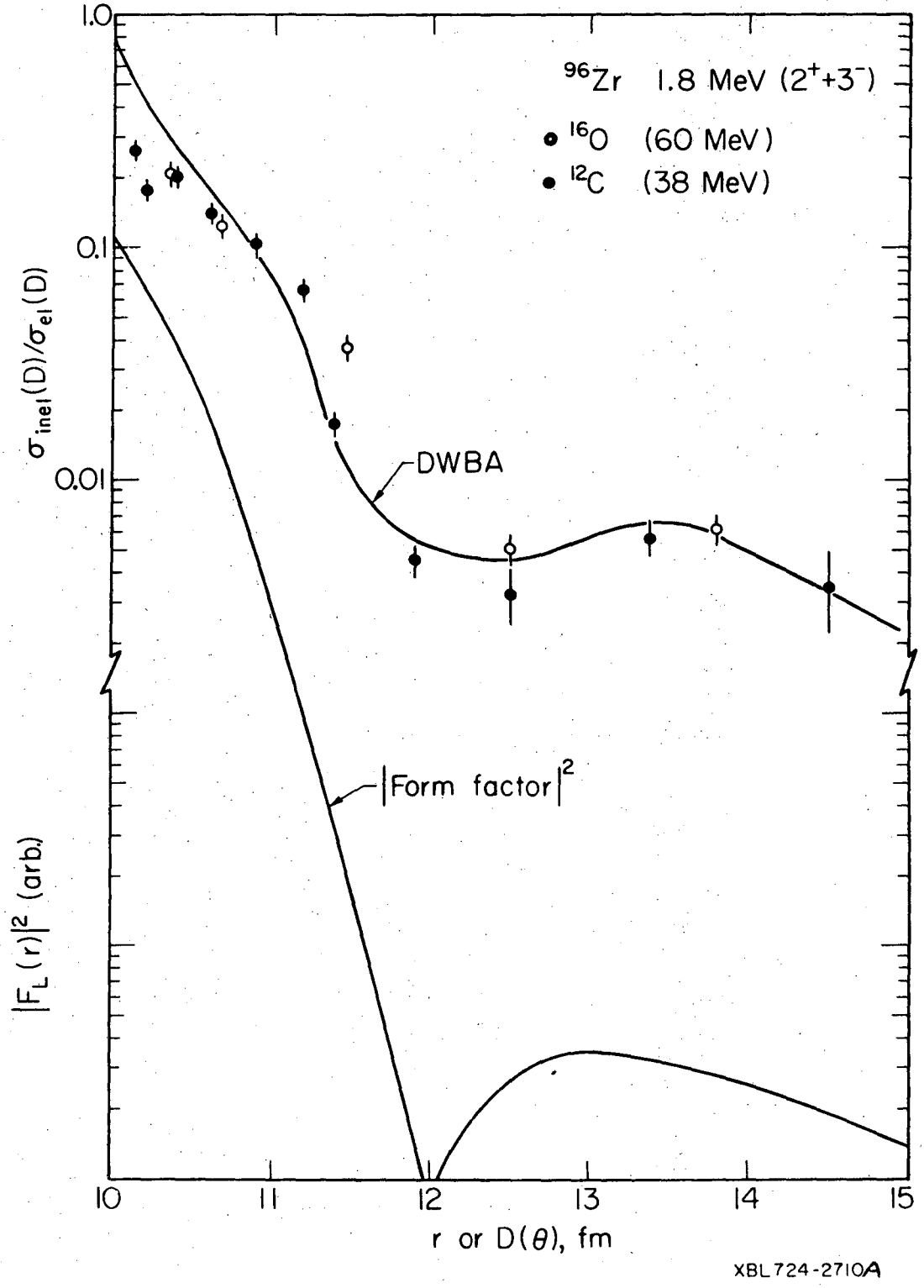
^{96}Zr 1.8 MeV (2^++3^-)
^{16}O (60 MeV)
^{12}C (38 MeV)
DWBA
|Form factor|^2
$\sigma_{inel}(D)/\sigma_{el}(D)$
$|F_L(r)|^2$ (arb.)
1.0
0.1
0.01
10
11
12
13
14
15
r or D(θ), fm
XBL724-2710A

Fig. 3

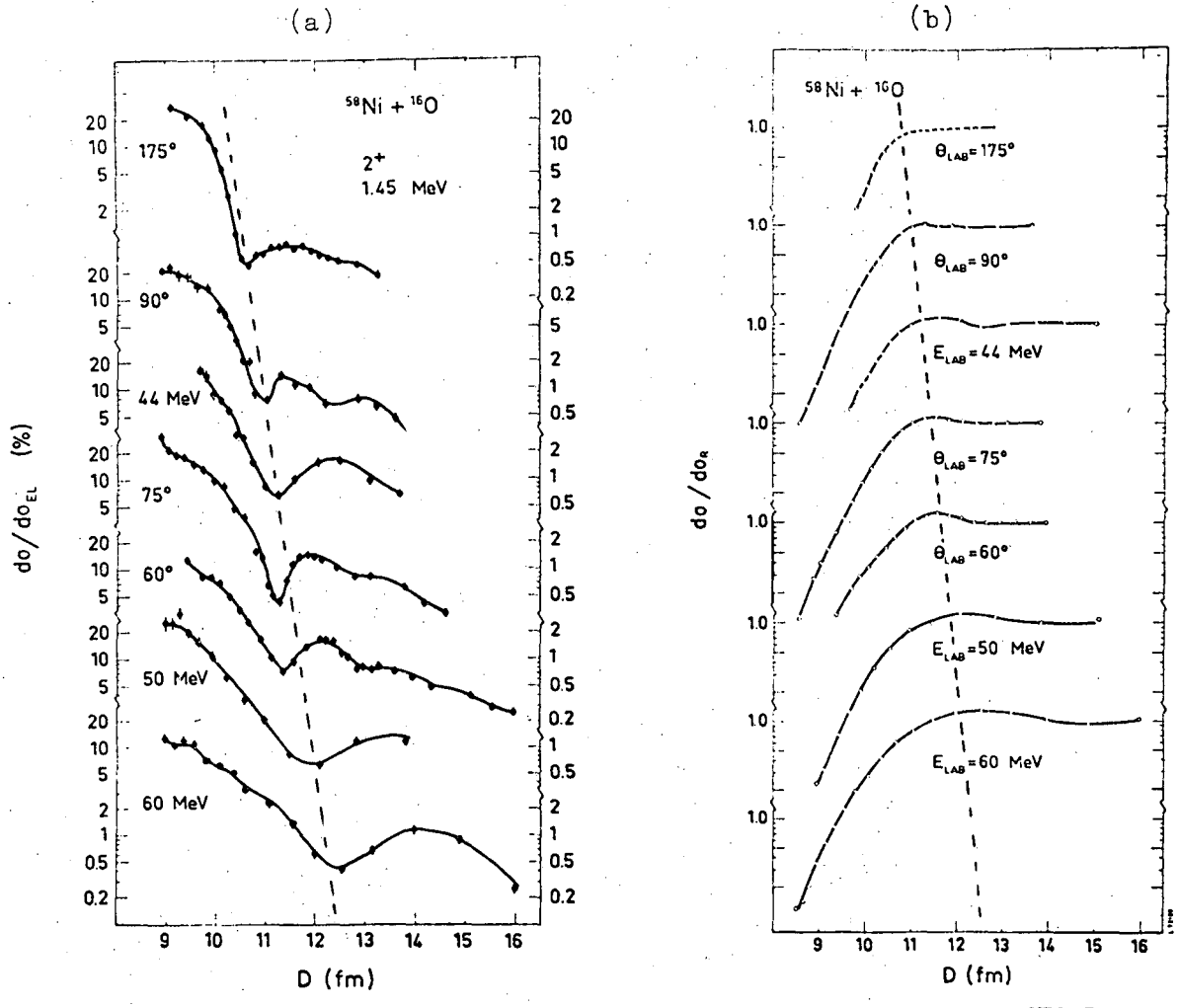
(a)
(b)
$^{58}Ni + ^{16}O$
2^+
1.45 MeV
175°
90°
44 MeV
75°
60°
50 MeV
60 MeV
$d\sigma/d\sigma_{EL}$ (%)
$d\sigma/d\sigma_R$
θ_{LAB}=175°
θ_{LAB}=90°
E_{LAB}=44 MeV
θ_{LAB}=75°
θ_{LAB}=60°
E_{LAB}=50 MeV
E_{LAB}=60 MeV
D (fm)
XBL 733-224

Fig. 4

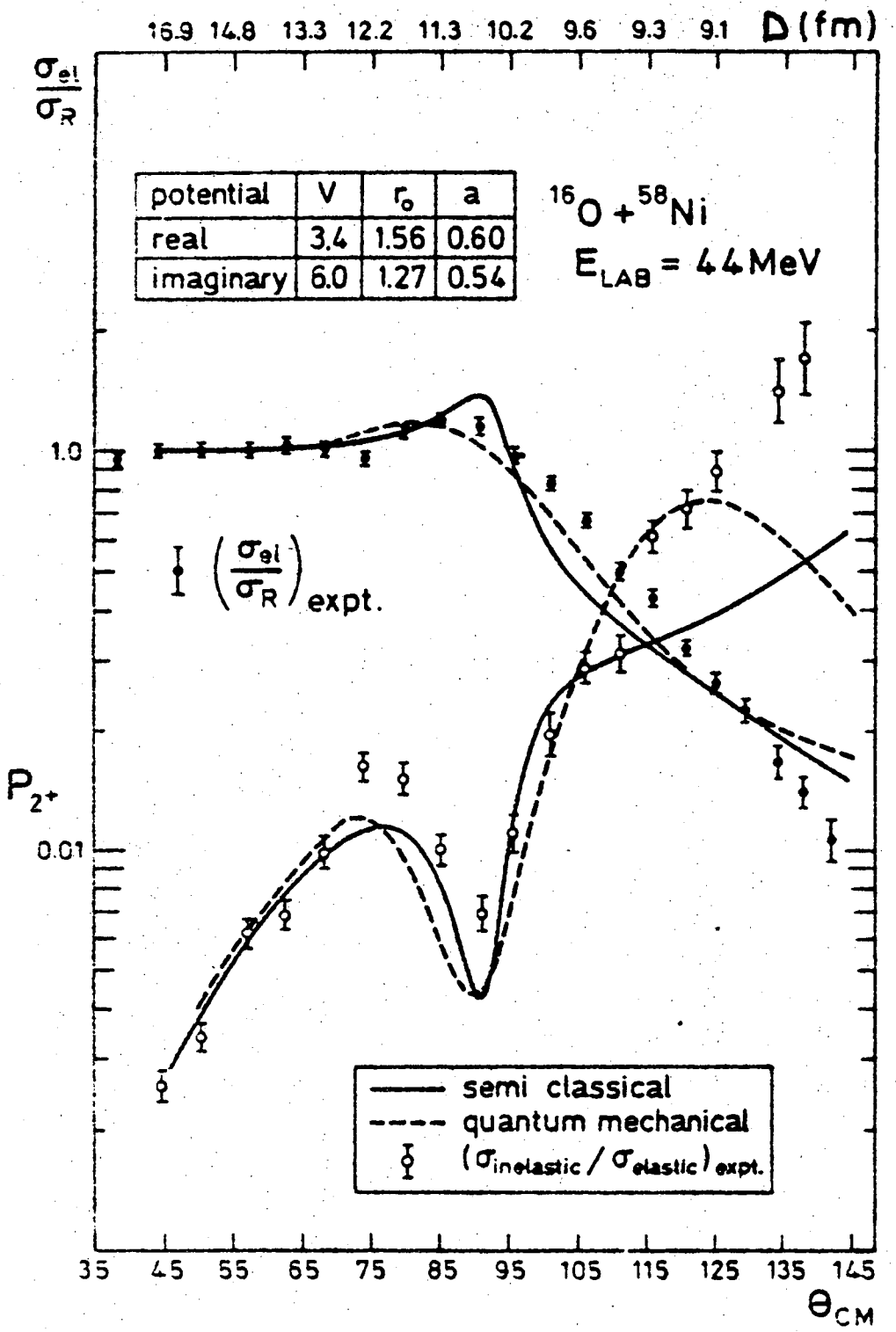

XBL 733-225

Fig. 5

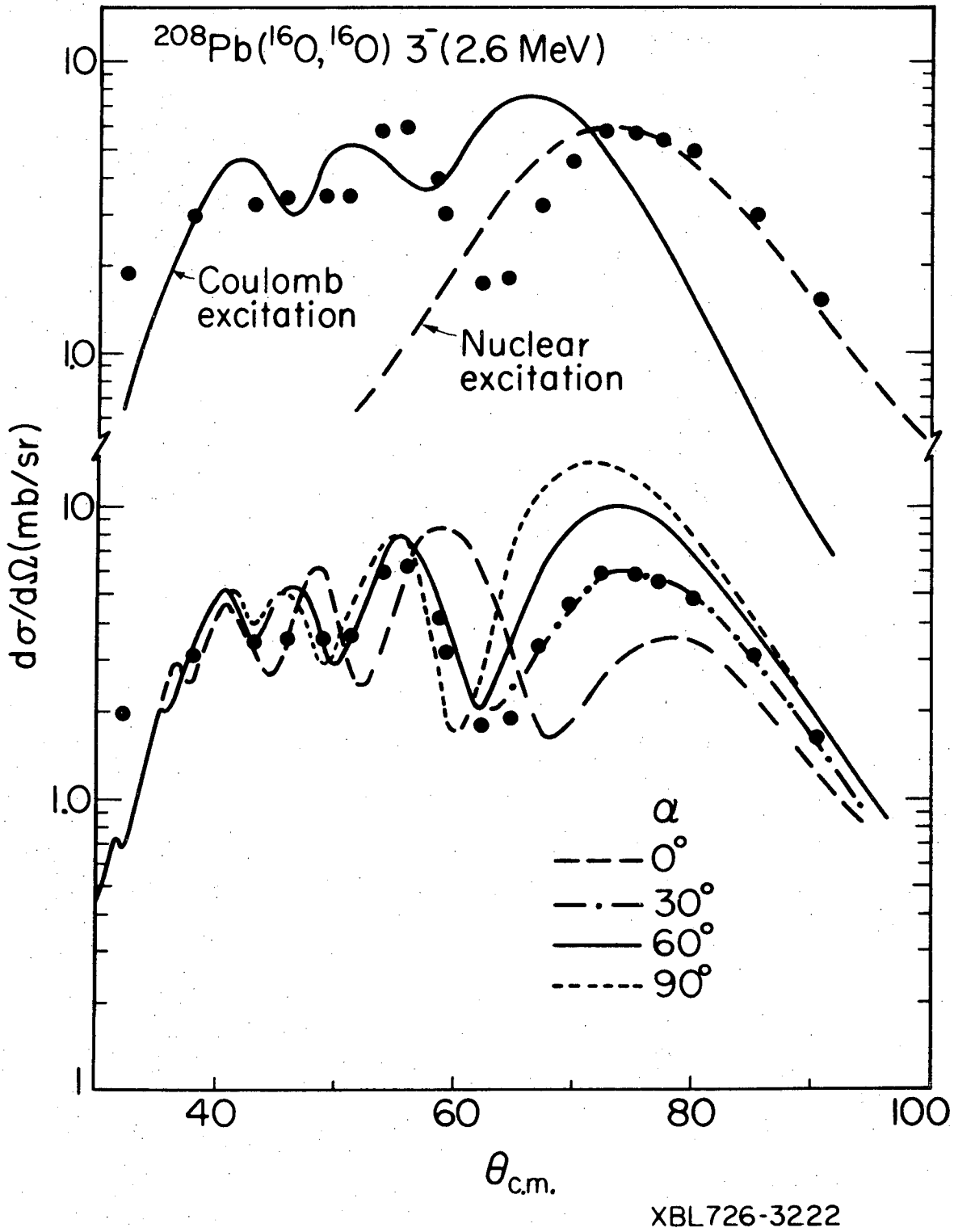
$^{208}Pb(^{16}O,^{16}O)\ 3^-(2.6\ MeV)$
Coulomb excitation
Nuclear excitation
$d\sigma/d\Omega$(mb/sr)
10
1.0
10
1.0
1
40
60
80
100
$\theta_{c.m.}$
α
0°
30°
60°
90°
XBL726-3222

Fig. 6

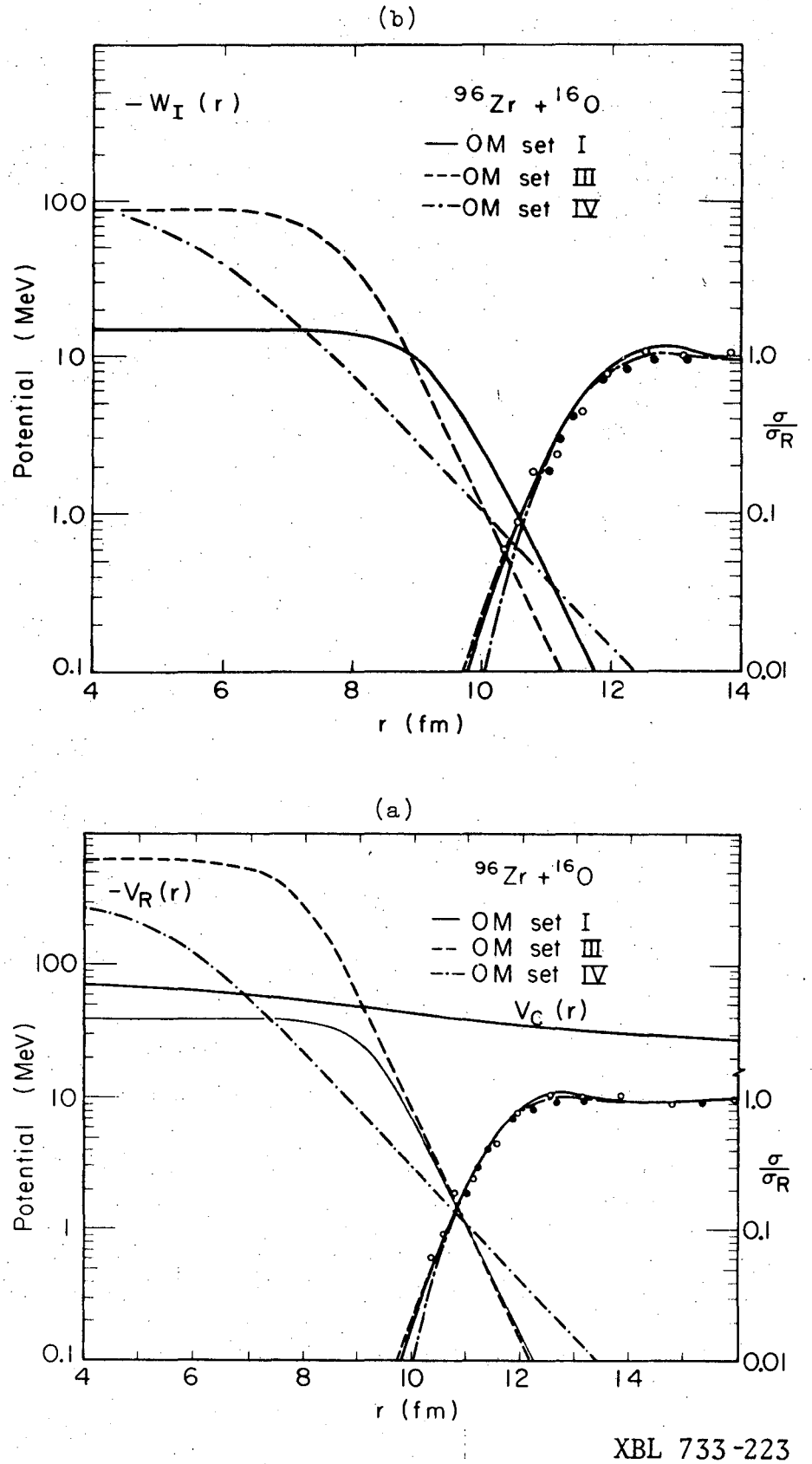
(b)
$-W_I(r)$
$^{96}Zr + ^{16}O$
OM set I
OM set III
OM set IV
Potential (MeV)
100
10
1.0
0.1
4
6
8
10
12
14
r (fm)
1.0
0.1
0.01
$\frac{\sigma}{\sigma_R}$
(a)
$-V_R(r)$
$^{96}Zr + ^{16}O$
OM set I
OM set III
OM set IV
$V_C(r)$
Potential (MeV)
100
10
1
0.1
4
6
8
10
12
14
r (fm)
1.0
0.1
0.01
$\frac{\sigma}{\sigma_R}$
XBL 733-223

Fig. 7

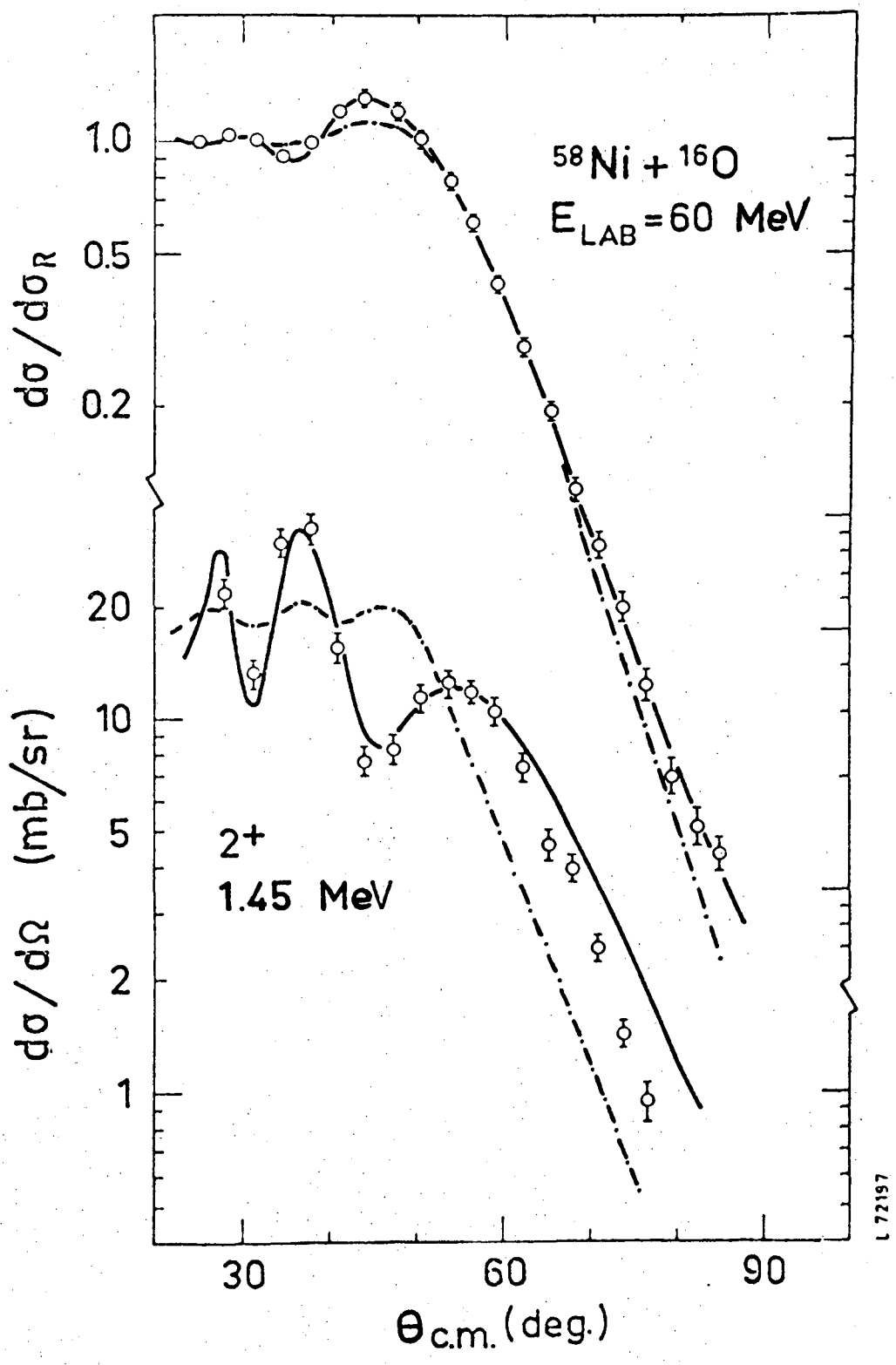

XBL 733-230

Fig. 8

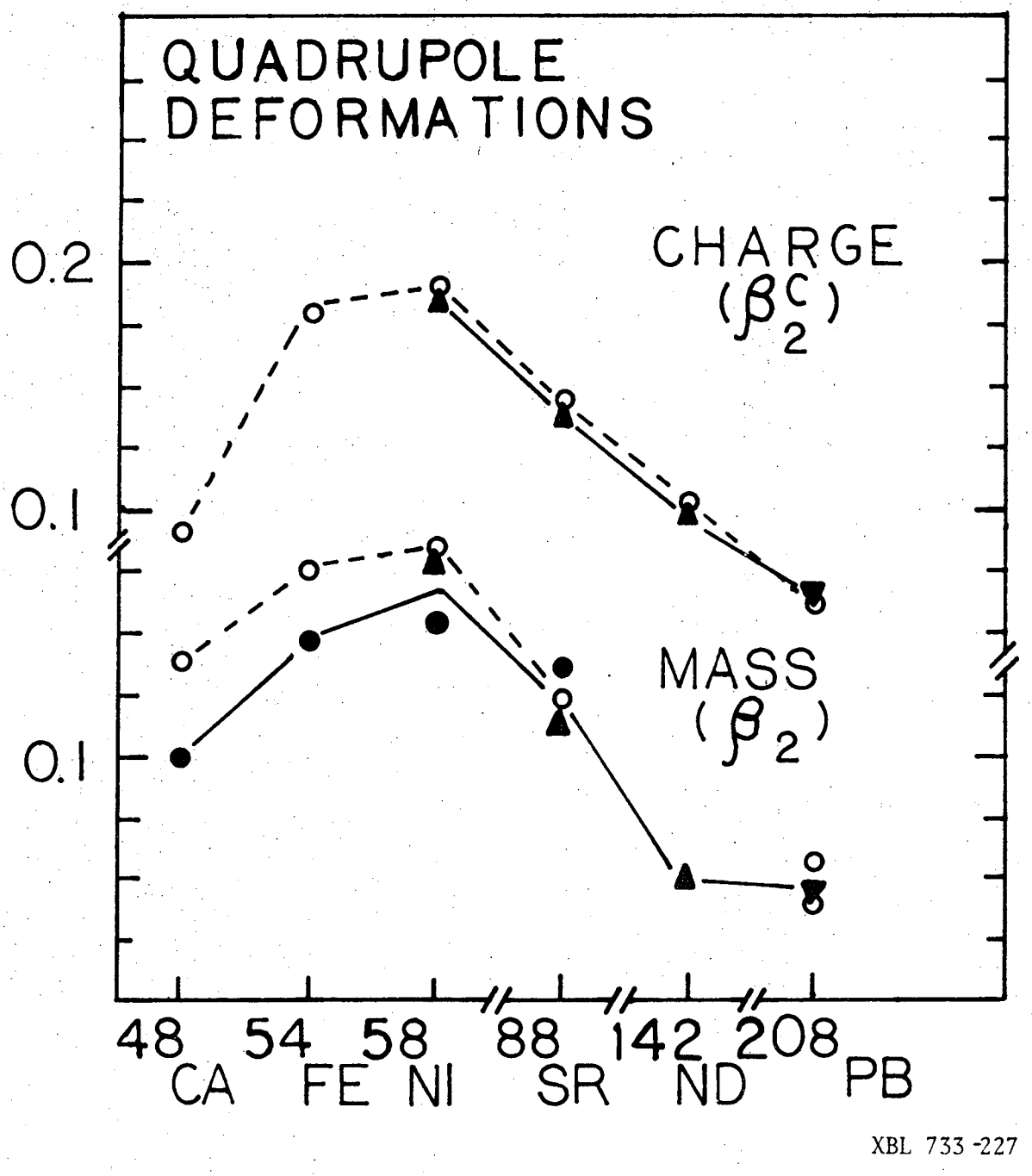

XBL 733-227

Fig. 9

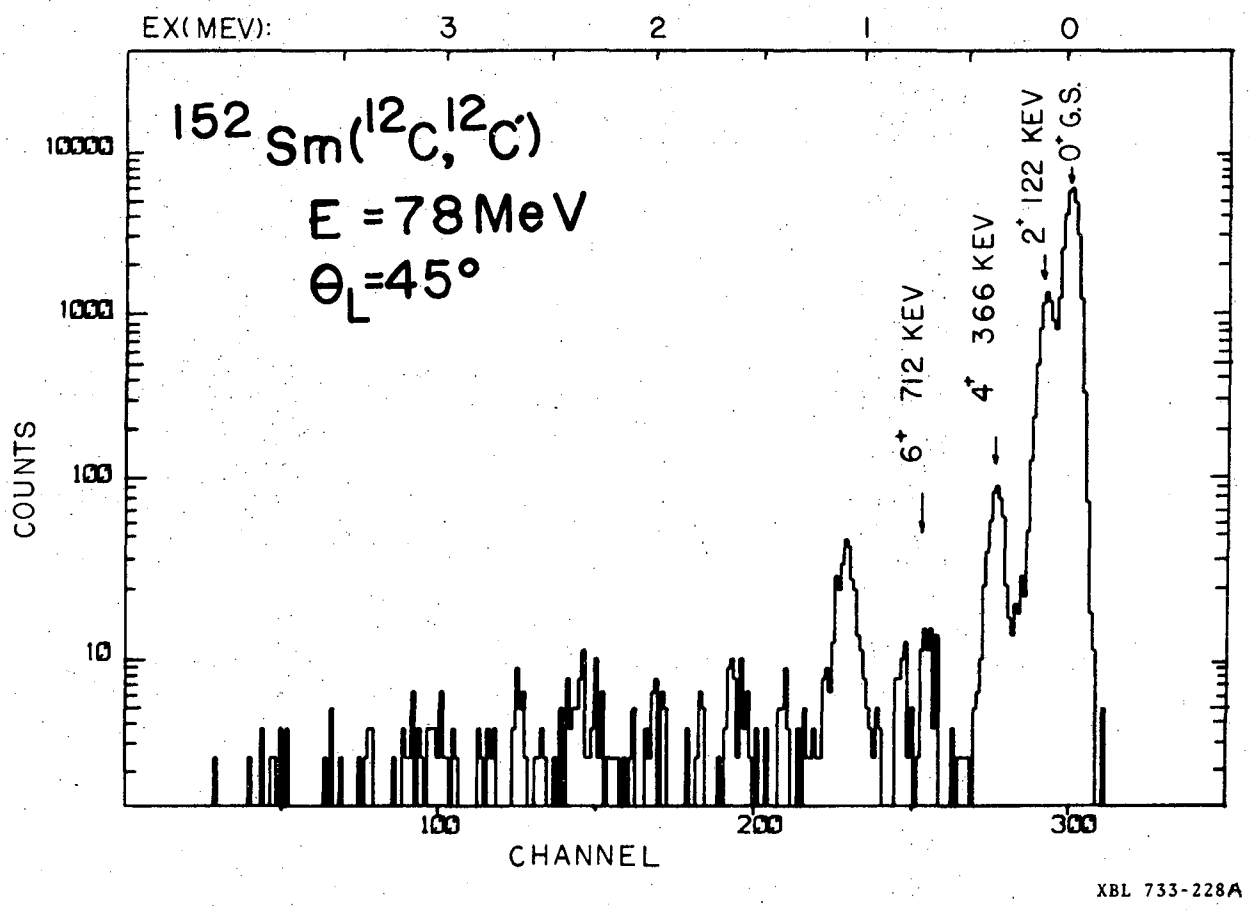
EX(MEV):
3
2
1
0
$^{152}Sm(^{12}C,^{12}C')$
E = 78 MeV
θ_L=45°
6⁺ 712 KEV
4⁺ 366 KEV
2⁺ 122 KEV
0⁺ G.S.
COUNTS
10000
1000
100
10
100
200
300
CHANNEL
XBL 733-228A

Fig. 10

TECHNICAL INFORMATION DIVISION
LAWRENCE BERKELEY LABORATORY
UNIVERSITY OF CALIFORNIA
BERKELEY, CALIFORNIA 94720